The spectrograms from whistlers observed by the Alouette satellite are very similar to those observed on the ground. This is perhaps unexpected, as whistlers were thought to be propagated strictly along magnetic field lines, only one of which would be intercepted by the satellite.

Broad bands of VLF noise, hiss, drawn chorus, etc., are also observed. These appear in a highly variable manner but do show evidence of magnetic field control. On the assumption that these emissions are caused by energetic particles whose velocity along the magnetic field approximately equals the velocity of propagation of VLF radio waves, the component of velocity along this field is appropriate to electrons with energies of the order of a few kiloelectron volts.

Energetic Particle Experiment

The six energetic particle counters contained in Alouette have characteristics as shown in Table 1.

Studies of the results of the first few months data from these counters have been carried out by McDiarmid et al.[8-11] These authors have discussed the observations made of the artificial radiation belts established by the "Starfish" test on July 9, 1962, and the Russian high-altitude nuclear tests in October and November of that year.[9] On one test, Alouette observed the initiation of a short-lived belt of electrons produced by one of the Russian tests.[10] The electrons were observed over Australia shortly after the test, but presumably they were dumped in the South Atlantic anomaly in the first circuit of the earth, as they were not observed on subsequent orbits.

One of the most interesting observations concerns the high flux of particles being dumped from the natural radiation zones at high latitudes. The energy input to the ionosphere from this source is significant, and it is reasonable to suppose that a number of ionospheric effects are due to this flux.[8, 11]

Conclusions

The experiments in the Alouette satellite have been most successful. A number of new results have been obtained, some of which lead to an appreciation of the importance of magnetic control of ionization in the ionosphere and the importance of the energy from the energetic particles dumped into the ionosphere from the radiation belts.

References

[1] Barrington, R. E. and Belrose, J. S., "Preliminary results from the very-low frequency receiver aboard Canada's Alouette satellite," Nature **198**, 651 (1963).

[2] Chapman, J. H., "Topside sounding of the ionosphere," Advan. Astronaut. Sci. **12**, 43 (1962).

[3] Chapman, J. H., "A survey of topside sounding of the ionosphere," *Proceedings of Commission III, Union Radio Scientifique Internationale, XIV General Assembly* (Elsevier Publishing Co., Inc., Amsterdam, Holland, to be published).

[4] Hartz, T. R., "The spectrum of galactic radio emissions between 1.5 and 10 mc/s as observed from a satellite," Nature **203**, 173 (1964).

[5] Hartz, T. R. and Roger, R. S., "The effective antenna beamwidth for a satellite-borne radio telescope," Can. J. Phys. (to be published).

[6] Lockwood, G. E. K. and Nelms, G. L., "Topside sounder observations of the equatorial anomaly in the 75°W longitude zone," J. Atomospheric Terrest. Phys. **26**, 569 (1964).

[7] Nelms, G. L., "Ionospheric results from the topside sounder Alouette," *Space Research IV* (North Holland Publishing Co., Amsterdam, 1963), Part III, p. 437.

[8] McDiarmid, I. B., Burrows, J. R., Budzinski, E. E., and Wilson, M. D., "Some average properties of the outer radiation zone at 1000 Kms," Can. J. Phys. **41**, 2064 (1963).

[9] McDiarmid, I. B., Burrows, J. R., Budzinski, E. E., and Rose, D. C., "Satellite measurements in the starfish artificial radiation zone," Can. J. Phys. **41**, 1332 (1963).

[10] Burrows, J. R. and McDiarmid, I. B., "A study of electrons artificially injected into the geomagnetic field in October 1962," Can. J. Phys. **42**, 1529 (1964).

[11] McDiarmid, I. B., Burrows, J. R., Rose, D. C., and Wilson, M. D., "High latitude particle flux measurements from the Satellite 1962 Beta Alpha (Alouette)," *Space Research IV* (North Holland Publishing Co., Amsterdam, 1963), Part III, p. 606.

[12] Molozzi, A. R., "Instrumentation of the ionospheric sounder contained in the Satellite 1962 Beta Alpha (Alouette)," *Space Research IV* (North Holland Publishing Co., Amsterdam, 1963), Part III, 413.

Application of Biot's Variational Method to Convective Heating of a Slab

HUGH N. CHU*
North American Aviation, Inc., Canoga Park, Calif.

Introduction

BIOT, in his paper[1] on the application of the variational principle to transient heat conduction problems, has discussed in detail examples involving prescribed surface temperatures. Subsequently, Lardner[2] applied Biot's method to problems for which the heat flux is prescribed. In this paper, we consider a semi-infinite slab and extend Biot's method to problems with a coupled convective boundary condition of the form

$$U(\theta_0 - \theta) = -k(\partial\theta/\partial x) \qquad (1)$$

at $x = 0$. Here x is the distance of a point in the semi-infinite slab from its surface, U the heat-transfer coefficient of the convection stream, θ_0 the temperature of the stream (assumed constant), k the thermal conductivity of the slab, and θ is the temperature in the slab (see Fig. 1). Models of this type have important applications to many convection heating problems, such as that one encountered in rocket engine nozzles where heat is transferred convectively from the hot gas stream to the nozzle wall.

Rough Approximation and Its Comparison with the Exact Solution

The approximate solution[1] for a semi-infinite slab with a prescribed boundary temperature θ_0 is

$$\theta = \theta_0[1 - (x/q_1)]^2 \qquad q_1 = 3.36(kt/c_v)^{1/2} \qquad (2)$$

The penetration depth q_1 is a generalized coordinate in the variational formulation used by Biot. For the convection condition of the present example, Eq. (1), the temperature at $x = 0$ is θ_1, which starts from zero at $t = 0$, then increases and eventually reaches θ_0 at $t = \infty$. A naturally convenient first approximation suggested by Eq. (2) is

$$\theta = \theta_1[1 - (x/q_1)]^2 \qquad q_1 = 3.36(kt/c_v)^{1/2} \qquad (3)$$

where the new unknown temperature θ_1 in Eq. (3) may be determined from the boundary condition, Eq. (1). The result is

$$\theta_1 = \theta_0[1 + (2k/Uq_1)]^{-1} \qquad (4)$$

The approximation used for Eq. (3) implies that the growth of q_1 is not affected by the variation of temperature at $x = 0$. For large times, when the time rate of increase of θ_1 is no longer appreciable, this assumption will be physically reasonable. However, the assumption is certainly inappropriate for small times. Since condition (1) tends to that of the prescribed boundary temperature as $U \to \infty$, approximation (3) is expected to be good for large U. To determine the

Received June 22, 1964.

* Senior Technical Specialist, Research Department, Rocketdyne Division. Member AIAA.

accuracy of approximaton (3), we compare it with the exact solution for $(Uq_1/2k) \ll 1$, or (equivalently) for $[(kt/c_v)^{1/2}U/2k] \ll 1$. This comparison will give us some idea of an upper bound for the error introduced by the approximation. The exact solution from Carslaw and Jaeger[3] is

$$\frac{\theta}{\theta_0} = \text{erfc}\left[\frac{x}{2}\left(\frac{kt}{c_v}\right)^{-1/2}\right] - \exp\left[\frac{Ux}{k} + \left(\frac{U}{k}\right)^2 \frac{kt}{c_v}\right] \times \text{erfc}\left[\frac{x}{2}\left(\frac{kt}{c_v}\right)^{-1/2} + \frac{U}{k}\left(\frac{kt}{c_v}\right)^{1/2}\right] \quad (5)$$

At the face of the slab, Eq. (5) reduces to

$$\left(\frac{\theta}{\theta_0}\right)_{x=0} = 1 - \exp\left[\left(\frac{U}{k}\right)^2 \frac{kt}{c_v}\right]\text{erfc}\left[\frac{U}{k}\left(\frac{kt}{c_v}\right)^{1/2}\right] \quad (6)$$

and when $[(kt/c_v)^{1/2}U/2k] \ll 1$, Eq. (6) can be written approximately

$$\left(\frac{\theta}{\theta_0}\right)_{x=0} = 1 - \left[1 + \left(\frac{U}{k}\right)^2 \frac{kt}{c_v} + \ldots\right]\left[1 - \frac{2}{(\pi)^{1/2}}\frac{U}{k}\left(\frac{kt}{c_v}\right)^{1/2} + \ldots\right] \approx 1.13\,\frac{U}{k}\left(\frac{kt}{c_v}\right)^{1/2} \quad (7)$$

Eliminating the temperature θ_1 from Eqs. (3) and (4), we find

$$\left(\frac{\theta}{\theta_0}\right)_{x=0} \approx 1.68\,\frac{U}{k}\left(\frac{kt}{c_v}\right)^{1/2} \quad (8)$$

a result nearly 50% higher than the exact value of Eq. (7). We next improve the approximation by considering the change of q_1 caused by the variation of θ_1.

Improved Approximation

In Biot's method, the functions V, D, and Q_j are to be determined so that the Lagrangian equations

$$(\partial V/\partial q_j) + (\partial D/\partial \dot{q}_j) = Q_j \quad (9)$$

are satisfied. The method can be applied to the entire body in question (or any part of it), and instantaneously, or in any arbitrary time interval.

For the present problem, we apply the variational method to the region $0 \leq x \leq q_1$ instantaneously. Retaining the parabolic temperature profile of (3), i.e., $\theta = \theta_1[1 - (x/q_1)]^2$, we find the heat flow vector H to be

$$H = (c_v/3)\theta_1 q_1[1 - (x/q_1)]^3 \quad (10)$$

and its time derivative is

$$\dot{H} = (c_v/3)[1 - (x/q_1)]^3(\dot{\theta}_1 q_1 + \theta_1 \dot{q}_1) + c_v\theta_1\dot{q}_1(x/q_1)[1 - (x/q_1)]^2 \quad (11)$$

Therefore, the following can be calculated:

$$D = (13/630)(c_v^2/k)\theta_1^2 q_1 \dot{q}_1^2 + (1/126)(c_v^2/k)\dot{\theta}_1^2 q_1^3 + (1/42)(c_v^2/k)q_1^2\dot{q}_1\theta_1\dot{\theta}_1 \quad (12)$$

$$V = (c_v/10)q_1\theta_1^2 \qquad Q_1 = (c_v/3)\theta_1^2$$

and the Lagrangian equation then yields

$$(1/10) + (13/315)(c_v/k)q_1\dot{q}_1 + (1/42)(c_v/k)(q_1^2\dot{\theta}_1/\theta_1) = \tfrac{1}{3} \quad (13)$$

On the other hand, differentiating Eq. (4) with respect to time, we obtain

$$(q_1^2\dot{\theta}_1/\theta_1) = 2\dot{q}_1 k/[U + (2k/q_1)] \quad (14)$$

Combining Eqs. (13) and (14), the single equation for determining q_1 is

$$\{(13/105) + (1/14)[2k/(2k + Uq_1)]\}q_1\dot{q}_1 = (7/10)(k/c_v) \quad (15)$$

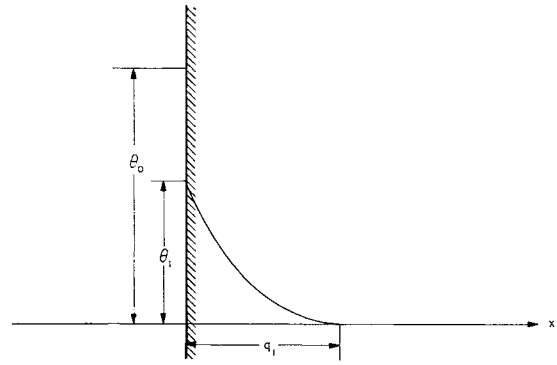

Fig. 1 Convection heating problem schematic.

If $Uq_1/2k \gg 1$, Eq. (15) reduces to

$$(13/105)q_1\dot{q}_1 = (7/10)(k/c_v)$$

which gives $q_1 = 3.36(kt/c_v)^{1/2}$, using the condition $q_1 = 0$ at $t = 0$. This result verifies our previous comments for the case of $Uq_1/2k \gg 1$.

On the other hand, if $Uq_1/2k \ll 1$, Eq. (15) simplifies to

$$[(13/105) + (1/14)]q_1\dot{q}_1 = (7/10)(k/c_v) \quad (16)$$

which gives $q_1 = 2.66(kt/c_v)^{1/2}$, under the condition $q_1(0) = 0$. Using the result in Eq. (4) we obtain

$$(\theta_1/\theta_0) = 1.33(U/k)(kt/c_v)^{1/2} \quad (17)$$

a value about 17% higher than the exact value of Eq. (7). The error has been reduced to $\frac{1}{3}$ of the previous approximation, which ignored the effect of the variation of θ_1 with q_1.

Further Improved Approximations

We note that the solutions (7, 8, and 17) are meant to describe the initial stages of growth of the boundary temperature θ_1. Solutions (8) and (17) were obtained by assuming the parabolic profile of temperature distribution, Eq. (3). This profile may not be appropriate for small times, since the growth of θ_1 tends to increase the curvature of the temperature profile. It is to be expected then that the error of an approximate approach can be further reduced by assuming, say, a cubic or higher degree approximation for the temperature profile.

For a cubic profile $\theta = \theta_1[1 - (x/q_1)]^3$, Eq. (4) is replaced by

$$\theta_1 = \theta_0[1 + (3k/Uq_1)]^{-1} \quad (18)$$

Differentiating (18) leads to

$$(q_1^2\dot{\theta}_1/\theta_1) = 3\dot{q}_1 k/[U + (3k/q_1)] \quad (19)$$

Applying the variational procedure for the cubic profile, we have

$$(1/14)q_1\dot{q}_1 + (1/24)(q_1^2\dot{\theta}_1/\theta_1) = (5/7)(k/c_v) \quad (20)$$

Combining Eqs. (19) and (20) yields

$$\{(1/14) + (1/24)[3k/(3k + Uq_1)]\}q_1\dot{q}_1 = (5/7)(k/c_v) \quad (21)$$

For small times, $Uq_1/3k \ll 1$, the solution of Eq. (21) is

$$q_1 = 3.56(kt/c_v)^{1/2} \quad (22)$$

and with Eq. (18) we obtain

$$(\theta_1/\theta_0) = 1.19(U/k)(kt/c_v)^{1/2} \quad (23)$$

Solution (23) is about 5% higher than the exact value of Eq. (7). This suggests that the result

$$\theta = \theta_0[1 - (x/q_1)]^3[1 + (3k/Uq_1)]^{-1} \qquad q_1 = 3.56(kt/c_v)^{1/2} \quad (24)$$

should be acceptable for small times. For large times, Eq. (21) yields $q_1 = 4.47(kt/c_v)^{1/2}$, an inordinately large value. However, for large times, a parabolic profile is a better approximation as we demonstrated earlier, so that solution (3) should be used for large times. For intermediate times, either Eq. (15) or Eq. (21) may be chosen. A precise criterion for selecting the appropriate transition point is beyond the scope of this paper. If both equations are used, that which leads to the lower value of q_1 is preferable, since both methods generally overestimate the exact value. Generally speaking, for smaller intermediate times, Eq. (21) should be used, whereas for larger intermediate times, Eq. (15) is preferable.

References

[1] Biot, M. A., "New methods in heat flow analysis with applications to flight structures," J. Aeronaut. Sci. **24**, 857–873 (1957).

[2] Lardner, T. J., "Biot's variational principle in heat conduction," AIAA J. **1**, 196–206 (1963).

[3] Carslaw, H. S. and Jaeger, J. C., *Conduction of Heat in Solids* (Oxford University Press, London, 1959), 2nd ed., p. 72.

Shock Reflection and Interaction at Hypersonic Speeds

SANNU MOLDER* AND EDWARD J. SZPIRO†
McGill University, Montreal, Canada

THIS note presents the results of a real-gas (air) calculation of the interaction of hypersonic oblique shock waves. The Mach number-altitude relationship used is representative of possible hypersonic ramjet flight capabilities. Detailed results for a range of wedge angles and Mach numbers have been obtained[1] for the dynamic and thermodynamic variables during and after the shock interaction and for the geometry of the interaction. Emphasis is placed upon conditions considered suitable for the use of the double oblique shock system as an intake for hypersonic ramjets which use supersonic combustion.

Mach [2] showed that, if a shock in an inviscid supersonic stream impinges on a plane wall, two flow geometries are possible, regular reflection and Mach reflection. Regular reflection occurs when an approaching flow is turned toward the wall by the incident shock and is then turned back by the reflected shock to the freestream direction. For Mach reflection, the incident shock must be stronger, thereby turning the flow more sharply toward the wall. If the deflection required to bring this flow to the freestream direction is larger than a critical angle,[3] then the reflected shock will tend to detach. However, detachment cannot occur because of the incident shock's presence; instead a three-shock configuration appears. A normal shock extends some distance up from the surface; it then divides into an incident and a reflected shock. The flow behind the normal shock is subsonic, whereas that behind the reflected shock is supersonic. These two flow regions are separated by a shear layer originating at the intersection of the three shocks.

For inviscid flow, the wall may be considered to be a streamline of symmetry, in which case a mirror image of either of the preceding types of reflections may be thought of as occurring below this line. In this case, the shocks are interacting instead of reflecting. Again there exist two possible flow geometries, regular interaction and Mach interaction. An important difference between reflection and interaction of shocks is that the latter is free from the viscous effects of boundary layers. Tepe and Tabakoff[4] consider the wedge boundary-layer effect on interaction of unequal shocks for an ideal gas from Mach 6 to 20. The flow displacement due to the shear layer has not been considered.

Received June 11, 1964. This work was sponsored by the Defence Research Board of Canada, under Grant No. 9550-06.

* Assistant Professor of Mechanical Engineering. Member AIAA.

† Research Assistant, Department of Mechanical Engineering.

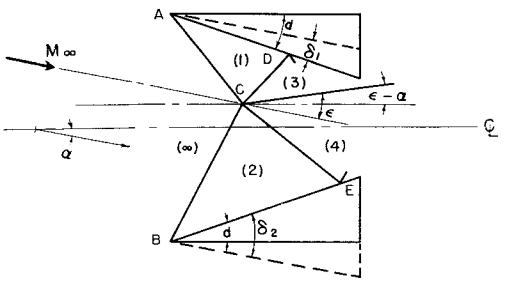

Fig. 1 Double-wedge intake with two interacting oblique shock waves.

The interaction of unequal shocks may be treated as a reflection problem, with the streamline through the interaction point no longer symmetrical, but deflected from the upstream flow by an angle ϵ. This deflected streamline separates two uniform flow regions that have undergone compressions through different shock systems but still retain identical flow directions and static pressures. The flow speed discontinuity gives rise to a high vorticity layer known as a contact surface or a slipline.

If two equal wedges of angle d are at an angle of attack α to the freestream flow, then the two wedges deflect the flow by unequal amounts. This is equivalent to having no angle of attack and the equivalent aerodynamic angles

$$\delta_1 = d - \alpha \qquad \delta_2 = d + \alpha \tag{1}$$

This regularly interacting shock system may be considered to act as a simple air intake for air-breathing propulsion systems.

Freestream conditions[5] were taken along the "boost path,"[6] which is a Mach number-altitude relationship, representative of possible hypersonic ramjet flight capabilities. The oblique shock characteristics across the first shocks are calculated by a method similar to Ref. 7 but using only one iteration. The conditions in regions 3 and 4 (Fig. 1) after the second shocks are obtained by requiring matched flow directions and equal static pressures. These conditions follow from the continuity and momentum equations, by considering the slipline as a streamline. The equivalent deflection angles for regions 3 and 4, i.e., the changes in flow direction before and after the second shocks, are

$$\delta_3 = \delta_1 + \epsilon \qquad \delta_4 = \delta_2 - \epsilon \tag{2}$$

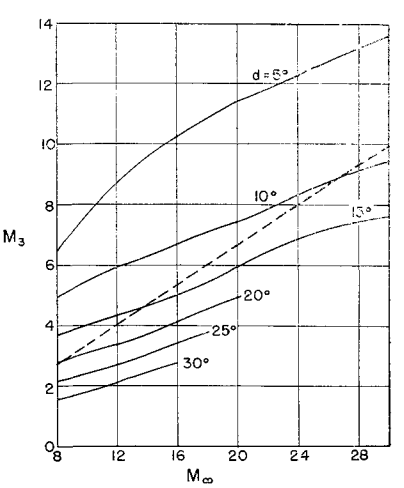

Fig. 2 M_3 vs M_∞ and d for $\alpha = 0°$.